Simple model for ablative stabilization

Karnig O. Mikaelian
University of California, Lawrence Livermore National Laboratory, Livermore, California 94550
(Received 3 June 1991; revised manuscript received 17 June 1992)

We present a simple analytic model for ablative stablization of the Rayleigh-Taylor instability. In this model the effect of ablation is to move the peak of the perturbations to the location of peak pressure. This mechanism enhances the density-gradient stabilization, which is effective at short wavelengths, and it also enhances the stabilization of long-wavelength perturbations due to finite shell thickness. We consider the following density profile: exponential blowoff plasma with a density gradient β, followed by a constant-density shell of thickness δt. For perturbations of arbitrary wave number k, we present an explicit expression for the growth rate γ as a function of k, β, and δt. We find that "thick" shells defined by $\beta\delta t \geq 1$ have $\gamma^2 \geq 0$ for any k, while "thin" shells defined by $\beta\delta t < 1$ can have $\gamma^2 < 0$ for *small* k, reflecting stability by proximity to the back side of the shell. We also present LASNEX simulations that are in good agreement with our analytic formulas.

PACS number(s): 52.35.Py, 47.20.−k, 52.40.Nk

I. INTRODUCTION AND MODEL

The suggestion that the Rayleigh-Taylor [1] (RT) instability at an ablating surface might grow at a rate γ which is smaller than the classical rate $\sqrt{gk}$ was made by Nuckolls *et al.* [2]. Here, g is the acceleration of a shell driven by ablation and k is the wave number $2\pi/\lambda$ for perturbations of wavelength λ. Experiments [3] performed so far are consistent with this idea, showing a reduction of about a factor of 2 from classical, though the situation is not completely clear; questions remain on how the quality of the laser beam affects the experimental results and over what wavelengths the reduction below classical is most effective [4]. On the theoretical side several models have been proposed [5] where the ablation velocity plays the key role. Numerical simulations [6] have shed some light on the complicated processes that occur at a distorted ablating surface, though a unique dispersion relation [$\gamma(k)$ versus k] has not yet emerged from simulations or theory.

Recent calculations [7] on Livermore's LASNEX code suggested that a density gradient, denoted by β, may play a role in ablative stabilization. The motivation for the model suggested here comes primarily from that observation and, to a smaller extent, from the question: Does the thickness δt of the shell appear in the dispersion relation?

Let us mention a case that had been a stumbling block to our mind in seeking a dispersion relation for $\gamma(k,\delta t,\beta)$. Taylor [1] treated the case of a single shell having a uniform density and free surfaces on each side. He found two eigenmodes: $\gamma^2=\pm gk$. The fast growing mode $\gamma=\sqrt{gk}$ is located at the "driven" surface, and the oscillating mode $\gamma=i\sqrt{gk}$ is located at the "back side." There is no δt dependence. We found that these modes are in fact present in *any* density profile as long as the surfaces are free [8]. Furthermore, the equation of state or the compressibility of the shell has no effect on the free-surface modes [9].

In the model presented here the apparent impasse that $\gamma^2=\gamma^2_{\text{classical}}=gk$ for any shell is circumvented by taking into account the density gradient which is present at the ablating surface, as shown in Fig. 1. Of course, density gradients are a classical effect which were first considered by Lord Rayleigh [1]. For an arbitrary density profile the growth rate is found by solving the equation

$$D(\rho DW)+\frac{gk^2}{\gamma^2}WD\rho-k^2\rho W=0\ . \tag{1}$$

In this equation, $W(y)$ is the perturbed fluid velocity (see, for example, Chandrasekhar [10]) and must be viewed as an eigenfunction to be found along with the associated eigenvalue for γ by solving Eq. (1) subject to appropriate boundary conditions. All other quantities in that equation are given: the density profile $\rho(y)$, the acceleration g, and the wave number k. D stands for the operator d/dy.

Multiplying Eq. (1) by W^m and integrating over y, we derived [11] a moment equation which is useful when Eq. (1) cannot be solved analytically or when a simple, albeit approximate, expression is sufficient. The approximation lies in using the classical eigenfunction $W_{\text{classic}}=e^{-k|y-y^*|}$ in the $m=0$ exact equation:

$$\frac{\gamma^2}{g}=\frac{\int WD\rho\,dy}{\int W\rho\,dy}\ . \tag{2}$$

This is the model proposed here, with the all-important stipulation that the location of the peak, y^*, be chosen according to the problem at hand, namely, a shell driven in the positive y direction with the plasma forming a gradient near the peak of the density profile (see Fig. 1). Since the pressure peaks at or near this peak, we will take $y^*=0$. This is the nonclassical element in our model which we believe is plausible.

To obtain an analytic expression, we will assume the following simple density profile, as indicated in Fig. 1:

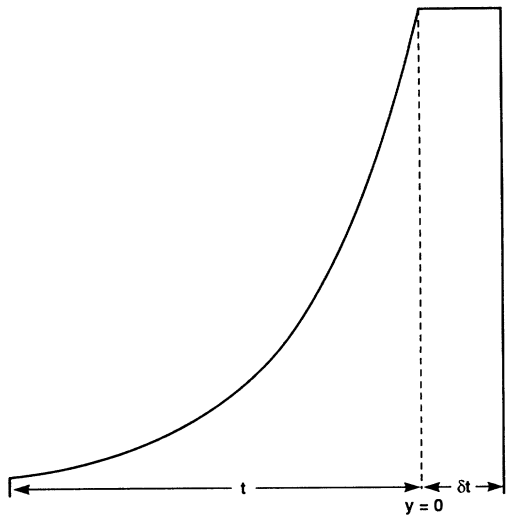

FIG. 1. The density profile of an ablatively driven target: low-density blowoff plasma of thickness t accelerating a high-density shell of thickness δt.

$$\rho(y)=\begin{cases}0\ , & y<-t\\ \rho_p e^{\beta y}\ , & -t\le y\le 0\\ \rho_p\ , & 0\le y\le \delta t\\ 0\ , & y>\delta t\ .\end{cases} \tag{3}$$

We refer to the region $-t\le y\le 0$ as the "blowoff" and the region $0\le y\le \delta t$ as the "shell." The "driven" surface is at $y=0$, and the "back side" is at $y=\delta t$.

Using $W=e^{-k|y|}$ and the above density profile in Eq. (2), we obtain

$$\frac{\gamma^2}{gk}=\frac{\beta-(\beta+k)e^{-k\,\delta t}}{k+(\beta+k)(1-e^{-k\,\delta t})}\ , \tag{4}$$

after setting the blowoff thickness $t=\infty$ (this is a good approximation because typical values are $t\ge 500$ μm. The result for finite t will be given in Sec. II).

The above model and variations thereof are discussed in Sec. II. In Sec. III we present LASNEX simulations and compare the numerical growth rates with our analytic formulas. Concluding remarks are given in Sec. IV.

II. DISCUSSION

As a check, note that in the limit $\beta\to\infty$ we recover Taylor's result: $\gamma^2\to gk$. Similarly, $\gamma^2\to -gk$ for $\delta t\to 0$. In the opposite limit where $\delta t\to\infty$, Eq. (4) reduces to

$$\frac{\gamma^2}{gk}=\frac{1}{1+2k/\beta}\ . \tag{5}$$

If we consider long-wavelength perturbations, i.e., $k\ll\beta$, Eq. (5) gives $\gamma^2\to gk$. This is not surprising since long-wavelength perturbations "ignore" the density gradient and grow classically. The *short-wavelength* limit of Eq. (5), however, is most interesting: $\gamma^2\to g\beta/2$. This is half the classical value for the exponential density profile (Rayleigh [1]), similarly for the density profile considered by Lelevier, Lasher, and Bjorklund [12] (see Ref. [13] for a comparison), and reflects the nonclassical element of the model: perturbations peaking at $y^*=0$. Classically, there *are* faster growing modes which typically peak at $y\approx -t/2$ and have $\gamma^2\to g\beta$ for both profiles [13]. In this admittedly very simple model, the effect of ablation is to shift the location of the peak from where it would classically grow fastest to the driven surface at $y=0$. This implies, of course, that if the perturbations were to peak inside the shell ($y^*>0$), then they would be even more stable; conversely, if they peak in the blowoff region ($y^*<0$), then they are less stable. We have verified this explicitly.

Having covered the $\delta t=0$ and the $\delta t=\infty$ limits, we now consider the finite δt case. We will find that Eq. (4) divides density profiles into two classes: "thick" and "thin," defined as $\beta\,\delta t\ge 1$ and $\beta\,\delta t<1$, respectively. We find that thick profiles always have $\gamma^2\ge 0$, while thin profiles can have $\gamma^2<0$. Obviously, these two classes are found by setting $\gamma^2=0$ in Eq. (4), and we get

$$1+k/\beta=e^{k\,\delta t}\ . \tag{6}$$

Viewing k as the independent variable in this equation, a solution other than $k=0$ exists if and only if the slope of the left-hand side (lhs) (a straight line) is greater than the slope of the right-hand side (rhs) (an exponential) at $k=0$. Therefore, a zero exists if and only if $1/\beta>\delta t$, which we call a thin profile. Otherwise, $\gamma^2>0$ always.

The reduction of the growth rate below classical is $\gamma/\sqrt{gk}$, and we plot it in Fig. 2 using Eq. (4). Three thick profiles ($\beta\,\delta t=5$, 10, and 20) and one thin profile ($\beta\,\delta t=\frac{1}{2}$) are used for illustration. The reduction at large

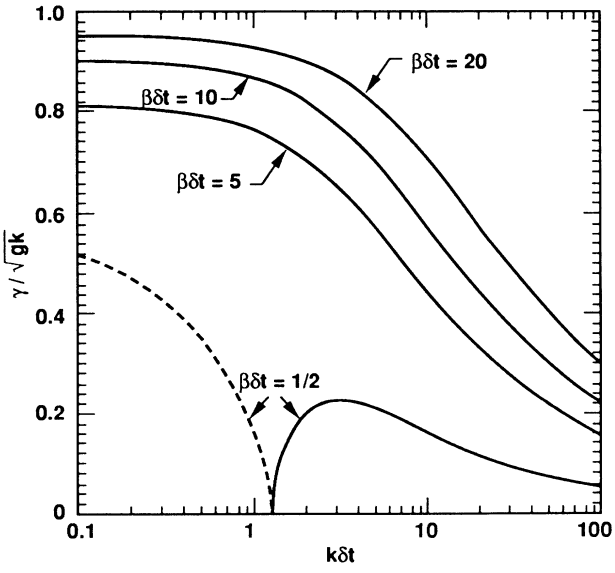

FIG. 2. $\gamma/\sqrt{gk}$, the ratio of the growth rate γ to its classical value $\sqrt{gk}$, plotted as a function of $k\,\delta t$ for $\beta\,\delta t=\frac{1}{2}$ (thin shell) and $\beta\,\delta t=5$, 10, and 20 (thick shells), using Eq. (4). The dashed line indicates that γ is imaginary below a cutoff wave number k_c given by Eq. (6). For the case $\beta\,\delta t=\frac{1}{2}$, one finds $k_c\delta t\approx 1.25$.

k is a result of density-gradient stabilization enhanced, as we have discussed, by ablation "dictating" the location of peak W. There is some stabilization at small k also, and this is due to the presence of the stable back side of the target. We identify it as a finite shell-thickness effect. Since long-wavelength, i.e., small-k, perturbations penetrate deeper into the shell (in our model, $W \sim e^{-ky}$), they sense the stabilizing effect of the back side more readily than the shorter-wavelength perturbations which are more localized near $y=0$. This "stability by proximity" is much more effective for the class of thin targets, so much so that for $k<k_c$, i.e., for wavelengths longer than a cutoff wavelength $\lambda_c=2\pi/k_c$, the perturbations are completely stable (the dashed curve in Fig. 2 indicates imaginary γ). The cutoff wave number k_c is of course given by Eq. (6) which can be easily, albeit numerically, solved. For $\beta\delta t=\frac{1}{2}$, it reads $1+2k_c\delta t=e^{k_c\delta t}$, whose solution is $k_c\delta t\approx 1.25$, as indicated in Fig. 2.

It is clear that, in our model, ablation stabilizes both short- *and* long-wavelength perturbations by bringing the peak of the perturbations closer to the back side. It has a modest (5–20 %) effect on long-wavelength perturbations in the thick shells of Fig. 2, but of course it has a dramatic effect on the thin shell.

The stability at long wavelengths is interesting but perhaps academic because most shells are thick. A typical example is $\delta t=10$ μm, $\beta^{-1}=3$ μm, $k^{-1}=8$ μm ($\lambda=50$ μm), for which Eq. (4) predicts $\gamma^2/gk\approx 0.45$, i.e., $\gamma\sim 67\%$ of $\gamma_{\text{classical}}$. The shell would have to be much thinner, or, equivalently, the density gradient much longer, for the $\lambda=50$-μm mode to be oscillatory.

An interesting variation is the profile where the shell density, instead of being constant and then dropping abruptly to zero as in Fig. 1, decreases linearly to zero, i.e., $\rho(y)$ is given by $\rho(y)=\rho_p(1-y/\delta t)$ in the range $0\le y\le\delta t$. Assuming that $y^*=0$ as before, the corresponding growth rate is found to be

$$\frac{\gamma^2}{gk}=\frac{\beta-(\beta+k)(k\,\delta t)^{-1}(1-e^{-k\,\delta t})}{\beta+2k-(\beta+k)(k\,\delta t)^{-1}(1-e^{1k\,\delta t})}\ , \tag{7}$$

which is somewhat more stabilizing than Eq. (4). For example, Fig. 2 shows $\gamma/\sqrt{gk}$ ranging from 16% to 81% for the $\beta\delta t=5$ case; Eq. (7) above gives 14–65 %. Setting $\gamma=0$, we find the cutoff wave number k_c, if there is one, from the solution of

$$1+\frac{\beta\delta t}{1-\beta\delta t+\beta k^{-1}}=e^{k\,\delta t}\ . \tag{8}$$

The analysis of this equation is more complicated than Eq. (6). It has a solution if and only if $1<\beta\delta t<2$. If $\beta\delta t\ge 2$, then γ^2 is always positive, which we called a "thick" profile. If $\beta\delta t\le 1$, then γ^2 is *always negative,* a feature absent from Eq. (4), which we may call a "superstable" profile. In the range $1<\beta\delta t<2$, Eq. (8) has a unique solution k_c so that, as in Eq. (4), $\gamma^2<0$ for $k<k_c$ and $\gamma^2>0$ for $k>k_c$.

To avoid any misconception, let us note that the growth rate or the oscillation frequency vanishes for $k\to 0$ where Eq. (4) reduces to

$$\frac{\gamma^2}{gk}=\frac{\beta\delta t-1}{\beta\delta t+1}\ , \tag{9a}$$

and Eq. (7) reduces to

$$\frac{\gamma^2}{gk}=\frac{\beta\delta t-2}{\beta\delta t+2}\ . \tag{9b}$$

In other words, the distinction between thick and thin shells determines whether $\gamma^2\to 0+$ or $0-$ as $k\to 0$.

Explicit expressions for γ calculated with a finite blowoff thickness t, with $y^*<0$, and $y^*>0$, can be found in Ref. [14], where we also present the exact solution of the classical problem for the profile given in Eq. (3). As expected from our discussion above, we find that there is less stabilization if $y^*<0$ and, conversely, more stabilization if $y^*>0$. The classical solution does not admit $y^*>0$.

Clearly, one can apply the same technique to other density profiles provided that the W in Eq. (2) is chosen judiciously. For the profile shown in Fig. 1, the model involves k, δt, and β, as given explicitly in Eq. (4) and, for a linearly decreasing ρ_{shell}, is given by Eq. (7). In Sec. III we compare these formulas with the results of direct numerical simulations using the hydrocode LASNEX [15].

III. LASNEX SIMULATIONS

We carried out two-dimensional LASNEX simulations of laser-driven plastic targets having single-wavelength perturbations, either on their back side, i.e., away from the laser, or at their ablation surface, similar to the calculations we reported earlier [7]. As in Ref. [7], we checked that the growth rates were independent of where the perturbation was initiated—perturbations feed through from one interface to the other. Additional checks involved independence of γ from initial amplitude η_0 in the linear regime, i.e., $\eta k\ll 1$, as well as the number of zones used to resolve a wavelength.

We consider first a 12.5-μm-thick CH target driven by a $\frac{1}{4}$-μm laser with intensity increasing linearly from 0 to 2×10^{13} W/cm^2 between $t=0$ and 1 ns, and held constant thereafter. Such a foil has an acceleration of about 36 μm/ns^2 after the shock breaks through. We considered wavelengths between 2.5 and 800 μm, so the classical growth rate $\sqrt{gk}$ ranges from 0.5 to 9.5 ns^{-1}. We saw reductions below classical with γ ranging from 28–80 % of classical. Our results are shown in Fig. 3(a). The continuous curve shown in that figure is Eq. (4) with $\delta t=10$ μm and $\beta^{-1}=2$ μm.

In Fig. 4 we overlay two snapshots of the density profile taken at $t=3$ and 5 ns. Although the profiles are not the same as in Fig. 1, nevertheless, the fit with the above values of δt and β is quite acceptable.

The second target was naturally the 25-μm-thick target considered in Ref. [7], driven by a laser with intensity increasing linearly from 0 to 2×10^{14} W/cm^2 between $t=0$ and 2 ns, and held constant thereafter (for details see Ref. [7]). The growth rates, normalized to $\sqrt{gk}$ where now $g\approx 100$ μm/ns^2, are shown in Fig. 3(b) as functions of $k\,\delta t$ where $\delta t=20$ μm. The continuous curve in that figure is Eq. (7) with $\delta t=20$ μm and $\beta^{-1}=1$ μm. An

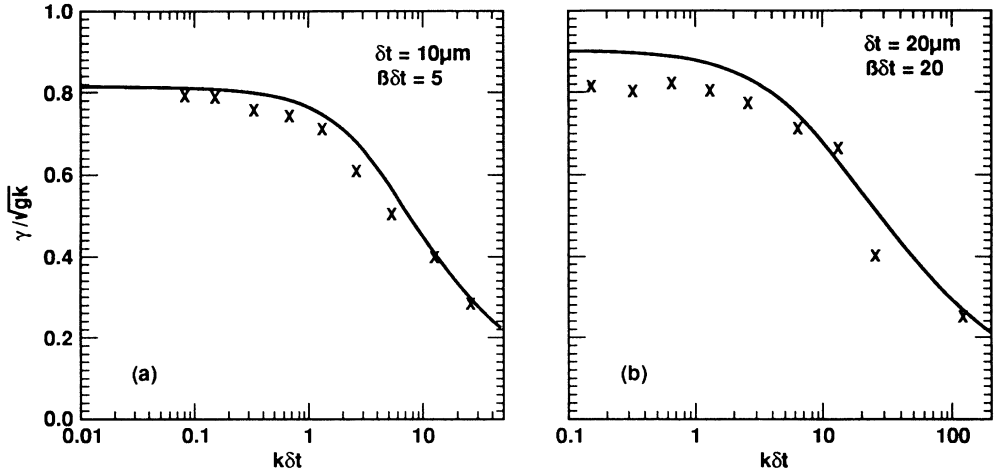

FIG. 3. $\gamma/\sqrt{gk}$ as a function of $k\,\delta t$ for (a) 12.5-μm CH foil driven at 2×10^{13} W/cm^2 and (b) 25-μm CH foil driven at 2×10^{14} W/cm^2. The latter target was also considered in Ref. [7]. LASNEX results are indicated by the crosses. The continuous curves in frames (a) and (b) come from Eqs. (4) and (7), respectively (see text).

equally good fit is Eq. (4) with $\beta^{-1}=2$ μm, i.e., the curve labeled $\beta\,\delta t=10$ in Fig. 2. The growth rates again range from 24–80 % of classical for $\lambda=1$ to 800 μm.

The growth rates for $\lambda=5$, 10, 20, 50, and 100 μm shown in Fig. 3(b) were reported earlier in Ref. [7]. As a check, we recalculated some of them because the LASNEX code is upgraded periodically. We found, within 2–3 %, the same results as before. In particular, the point at $\lambda=5$ μm ($k\,\delta t=25$) was repeated and again found to have $\gamma\approx4.5$ ns^{-1}, compared with 11.2 ns^{-1} classically. As discussed in Ref. [7], such very short-wavelength calculations require extremely long computations because of the needed resolution and radiation transport in LASNEX.

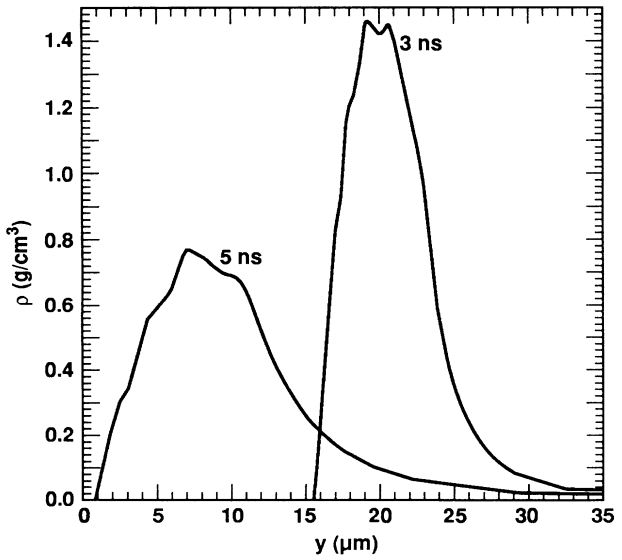

FIG. 4. Density profiles for the 12.5-μm-thick target at $t=3$ and 5 ns.

Several calculations, in the old as well as the new target, were repeated without radiation transport. As in Ref. [7], calculations including radiation transport exhibited smaller growth rates, particularly for shorter-wavelength perturbations. In fact, it was our explanation of this phenomenon in terms of longer density gradients [7] that led us to the model proposed in this paper, which can be described as an enhancement of the density-gradient stabilization via ablation.

The stabilization at long wavelengths appears naturally in our model as a finite shell-thickness effect and is seen in our simulations also, although it is only a 20% effect for these targets. In Fig. 5 we illustrate the evolution of a 800-μm-long perturbation with a 1-μm initial amplitude on the back side of the 25-μm plastic target. The lower half of the target is shown in each of the snapshots at $t=0$, 1, 2, 3, 4, and 5 ns. The expected phase reversal of the perturbation, its feed through to the ablation surface, and subsequent growth to a "ribbonlike" thin shell are all seen in these snapshots.

The strong coupling between the interfaces, viz., the back side away from the laser and the front side facing the laser, arises in long-wavelength perturbations and of course is the reason for the ribbonlike look in Fig. 5. Shorter-wavelength perturbations do not feed through as much—an example with $\lambda=20$ μm was shown in Ref. [7]. This is consistent with our model where

$$\eta\ (\text{back})/\eta\ (\text{front})=e^{-k\,\delta t}\ :$$

Since $k=2\pi/\lambda$, it follows that long-wavelength perturbations have η (back) $\approx\eta$ (front), while short-wavelength perturbations have η (back) $\ll\eta$ (front).

Other models do not describe the shape of the perturbation nor do they exhibit any dependence on shell thickness, so we can only compare their growth rates with ours, which we do in Sec. IV.

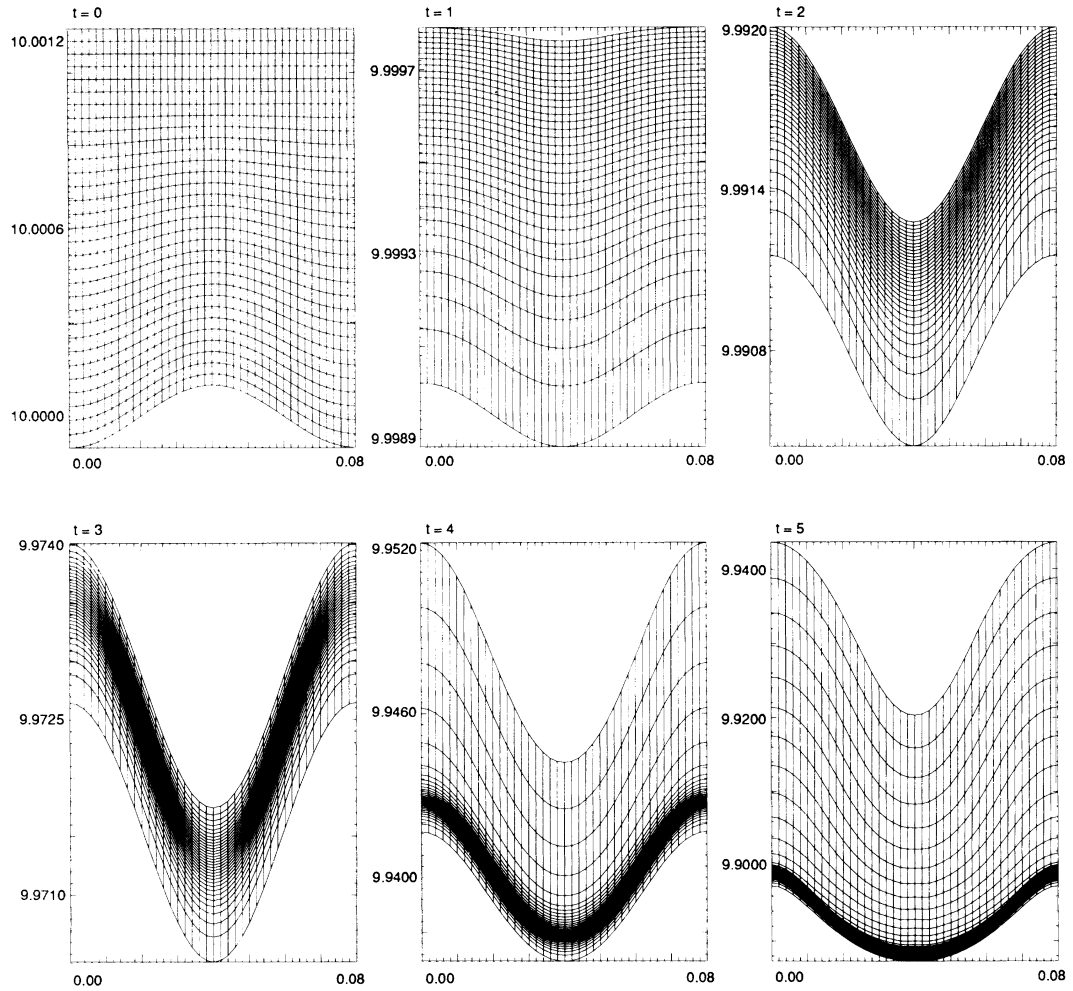

FIG. 5. Snapshots of the lower half of the 25-μm-thick target with a $\lambda=800$-μm, $\eta_0=1$-μm perturbation on its back side. The dimensions are in centimeters. The foil moves about 1 mm in 5 ns. The snapshots are at $t=0$, 1, 2, 3, 4, and 5 ns. The code is Lagrangian in the direction of motion and therefore the same fluid element, viz., the lower half of the target, is seen in each snapshot. The horizontal width is always 800 μm, while the vertical scale changes as the target undergoes compression, decompression, or ablation.

IV. COMPARISONS AND CONCLUDING REMARKS

We emphasize that Eq. (4) is only an extremely simple *model* for the complex process of ablative stabilization—only a shift in the location of peak W, as compared with the classical. It is true that the classical problem is also complex (see Ref. [14]), but a good approximation can be obtained provided we use Eq. (2) with a W peaking in the low-density blowoff region. The contrast with classical is best illustrated in the $\delta t=\infty$ limit: Equations (4) and (7) both reduce to Eq. (5):

$$\gamma^2=g\beta/(2+\beta/k)\ , \tag{10}$$

compared with the expression

$$\gamma^2=g\beta/(1+\beta/k) \tag{11}$$

describing the classical case [13].

Stability by proximity would predict that if one continues the ablation process and the shell is close to burning through, it may become so thin that long wavelengths may suddenly go stable. Alternatively, the peak may move away from the back side, i.e., $y^*<0$, and continue to grow there. As far as we know, neither phenomenon has ever been observed.

The modes seen in our LASNEX calculations peaked close to $y^*=0$, with the very short-wavelength modes moving somewhat away into the blowoff region. Of course, this is only a qualitative description because the density profiles are not identical to the one shown in Fig. 1, as can be seen by comparing it with Fig. 4. Other examples are given in Ref. [7]. Nevertheless, the computed growth rates are fairly well described by our model.

There are striking differences between this and other models of ablative stabilization, particularly at very long and very short wavelengths. Although the general trend is similar, viz., less stabilization at long wavelengths and more stabilization at short wavelengths, other models differ by predicting too little stabilization at long wavelengths and too much stabilization at short wavelengths.

As we mentioned in Ref. [7], the expression

$$\gamma=[gk\beta/(k+\beta)]^{1/2}-Vk \tag{12}$$

is also a good fit to our LASNEX results for intermediate wavelengths. This was an attempt to combine the classical density-gradient effect, Eq. (11), with Bodner's result [5],

$$\gamma=\sqrt{gk}-Vk\ , \tag{13}$$

where V is the ablation velocity. It is clear that these formulas predict 100% of classical for very long-wavelength perturbations, and this was the reason for extending our LASNEX simulations in this paper to the long wavelengths such as 800 μm (although the deviation was beginning to show even at the 100-μm wavelength in Ref. [7]). The fit for $5\leq\lambda\leq 50$ μm was quite acceptable, taking $\beta^{-1}=1$ μm and $V=2$ μm/ns.

The same remark applies also to other formulas such as

$$\gamma^2=gk-P_A k^2/\rho_p \tag{14}$$

or

$$\gamma=0.9\sqrt{gk}-3Vk\ , \tag{15}$$

where P_A is the ablation pressure (for a review, see Kull's report in Ref. [6]). The last formula above, proposed by Takabe *et al.* [5], predicts 90% of classical as $k\rightarrow 0$ and is closer to the 80% we find for these targets.

In the short-wavelength limit, i.e., for $k\rightarrow\infty$, Eqs. (12)–(15) predict that there is a cutoff beyond which all perturbations are stable. For Eq. (12),

$$k_c=\frac{\beta}{2}\left[\left[1+\frac{4g}{\beta V^2}\right]^{1/2}-1\right]\ , \tag{16}$$

and for Eq. (15),

$$k_c=0.09g/V^2\ . \tag{17}$$

Perturbations with $k>k_c$ are stable. In contrast, there is no such short-wavelength cutoff in our model. This was the reason for extending our LASNEX simulations to very short wavelengths. We found no stable perturbations, down to the 1-μm wavelength we can perform on LASNEX with reasonable accuracy and computer time.

Equations (16) and (17) predict $\lambda_c=2\pi/k_c=1.4$ and 2.8 μm, respectively, where we have used $g=100$ μm/ns^2, $V=2$ μm/ns, and $\beta^{-1}=1$ μm for our 25-μm target. Therefore, the 1-μm-long perturbation should have been absolutely stable. Our simulations, however, showed a positive growth rate at 24% of classical [see Fig. 3(b)], which compares favorably with our model: It predicts 20–28 % of classical for $\beta^{-1}=1$–2 μm (use $\gamma\approx\sqrt{g\beta/2}$). As we mentioned earlier, good resolution and radiation transport were necessary in such simulations. We had to start with a very small initial perturbation, $\eta_0=1$ Å, to stay in the linear regime and, more importantly, to be able to run the problem without early bowties. We believe the Lagrangian nature of the code was essential to suppress the numerical diffusion which might otherwise be present in a Eulerian hydrocode.

On the experimental side, the situation is somewhat confusing. Early experiments by Grun *et al.* [3] observed $\gamma=0$ for $\lambda=50$ μm. We have already described in Ref. [7] our failure to explain this result by LASNEX simulations (other codes also have trouble; see Grun *et al.* in Ref. [3]). We know of no other example where complete stability ($\gamma\leq 0$) was seen [16]. More recent experiments by Desselberger *et al.* [3] find about 20% of classical, within error bars, for $\lambda=50$ μm. The target and drive conditions were different. Unpublished results from NOVA experiments [17] cannot be adequately described by a growth rate, though they are not inconsistent with the assumption that $\gamma\approx 40$–70 % of classical for wavelengths between 20 and 70 μm [17]. As we mentioned above, such intermediate wavelengths can be fit by any of the four formulas in Eqs. (12) through (15).

To choose among the formulas or our model, one must go to extremes in wavelengths, both very long and very short: Is there some stabilization at $\lambda\gg\delta t$? This would speak for our model, i.e., stability by proximity [or one could simply adjust the constant 0.9 in Eq. (15), which is not in the spirit of this paper]. At the other extreme, is there a wavelength short enough that $\gamma<0$? This is the case, for example, with Eqs. (12) and (15) which asymptote to $-Vk$ and $-3Vk$, respectively. Finding such a short-wavelength cutoff would speak against our model where the asymptotes for $k\rightarrow\infty$ are $\sqrt{g\beta/2}$ and $\sqrt{(g\beta/2)(1-1/\beta\delta t)}$ from Eqs. (4) and (7), respectively.

Such extremes are, understandably, difficult to attain numerically and even more so experimentally. Other aspects of our model, such as interface coupling between the back and the front sides of the target, are also important but cannot be measured by the presently favored experimental technique, which is face-on x-ray radiography, even for long wavelengths where the effect is substantial.

We believe that the simple model presented in this paper has physical motivation and predictive power, inviting further research—both numerical and experimental. We have highlighted its differences with previous work to stimulate such activity and, we hope, to pin down the parameters affecting ablative stabilization.

ACKNOWLEDGMENT

This work was performed under the auspices of the U.S. Department of Energy by the Lawrence Livermore National Laboratory under Contract No. W-7405-ENG-48.

[1] Lord Rayleigh, *Scientific Papers* (Dover, New York, 1965), Vol. II, p. 200; G. I. Taylor, Proc. R. Soc. London Ser. A **201**, 192 (1950).

[2] J. Nuckolls, L. Wood, A. Thiessen, and G. Zimmerman, Nature **239**, 139 (1972).

[3] A. J. Cole *et al.*, Nature **299**, 329 (1982); R. R. Whitlock *et al.*, Phys. Rev. Lett. **52**, 819 (1984); J. Grun *et al.*, *ibid.* **58**, 2672 (1987); M. Desselberger *et al.*, *ibid.* **65**, 2997 (1990); B. A. Remington *et al.*, *ibid.* **67**, 3259 (1991).

[4] For example, early experiments reported no growth at

$\lambda = 50$ μm, contrary to more recent experiments (see J. Grun *et al.* and M. Desselberger *et al.* in Ref. [3]).

[5] S. E. Bodner, Phys. Rev. Lett. **33**, 761 (1974); K. A. Brueckner and S. Jorna, Rev. Mod. Phys. **46**, 325 (1974); D. B. Henderson, R. L. McCrory, and R. L. Morse, Phys. Rev. Lett. **33**, 205 (1974); H. Takabe *et al.*, Phys. Fluids **28**, 3676 (1985); H. J. Kull and S. I. Anisimov, *ibid.* **29**, 2067 (1986); A. Bud'ko and M. A. Liberman, Phys. Rev. Lett. **68**, 178 (1992).

[6] J. D. Lindl and W. C. Mead, Phys. Rev. Lett. **34**, 1273 (1975); C. P. Verdon *et al.*, Phys. Fluids **25**, 1653 (1982); M. H. Emery, J. H. Gardner, and S. E. Bodner, Phys. Rev. Lett. **57**, 703 (1986); **62**, 694(E) (1989); M. Tabak, D. H. Munro, and J. D. Lindl, Phys. Fluids B **2**, 1007 (1990); H. Sakagami and K. Nishihara, Phys. Rev. Lett. **65**, 432 (1990); J. H. Gardner, S. E. Bodner, and J. P. Dahlburg, Phys. Fluids B **3**, 1070 (1991). For a review, see H. J. Kull, Phys. Rep. **206**, 197 (1991).

[7] K. O. Mikaelian, Phys. Rev. A **42**, 4944 (1990).

[8] K. O. Mikaelian, Phys. Rev. Lett. **48**, 1365 (1982); Phys. Rev. A **26**, 2140 (1982).

[9] N. A. Inogamov, Prikl. Mekh. Tekh. Fiz. **5**, 110 (1985).

[10] S. Chandrasekhar, *Hydrodynamic and Hydromagnetic Stability* (Oxford University Press, London, 1968).

[11] K. O. Mikaelian, Phys. Rev. A **33**, 1216 (1986).

[12] R. Lelevier, G. J. Lasher, and F. Bjorklund, University of California Report No. UCRL-4459, 1955 (unpublished), available from the Technical Information Department, Lawrence Livermore National Laboratory, Livermore, CA 94550.

[13] K. O. Mikaelian, Phys. Rev. A **40**, 4801 (1989).

[14] K. O. Mikaelian, University of California Report No. UCRL-JC-107355, 1991 (unpublished).

[15] G. B. Zimmerman and W. L. Kruer, Comments Plasma Phys. Controlled Fusion **2**, 85 (1975).

[16] Early experiments [A. Raven *et al.*, Phys. Rev. Lett. **47**, 1049 (1981)] reported no growth in 3-μm-thick targets. Subsequent experiments with 3-μm-thick targets reported 30% of classical at $\lambda = 20$ μm (Cole *et al.* in Ref. [3]).

[17] S. G. Glendinning (unpublished).

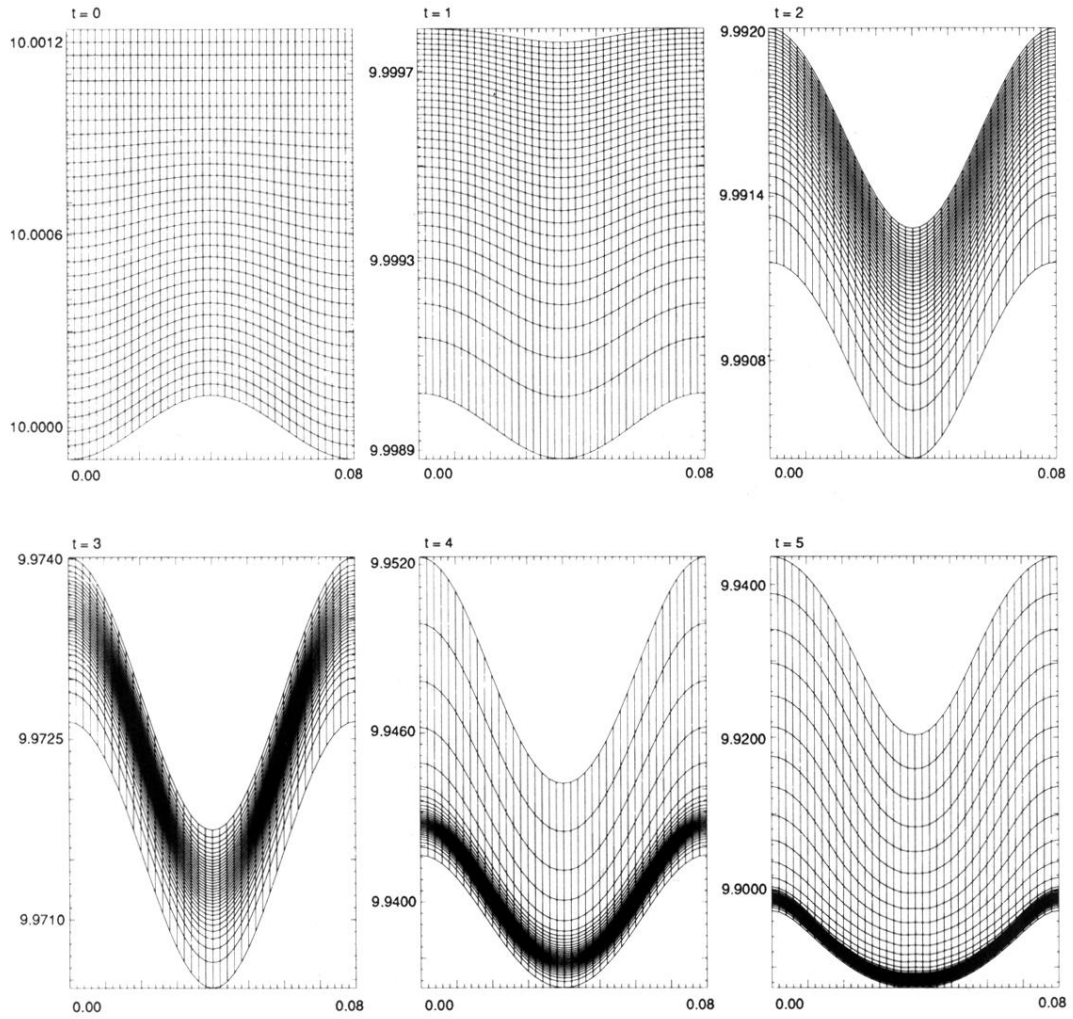

FIG. 5. Snapshots of the lower half of the 25-μm-thick target with a $\lambda = 800$-μm, $\eta_0 = 1$-μm perturbation on its back side. The dimensions are in centimeters. The foil moves about 1 mm in 5 ns. The snapshots are at $t = 0$, 1, 2, 3, 4, and 5 ns. The code is Lagrangian in the direction of motion and therefore the same fluid element, viz., the lower half of the target, is seen in each snapshot. The horizontal width is always 800 μm, while the vertical scale changes as the target undergoes compression, decompression, or ablation.